

Preferential uptake of SARS-CoV-2 by pericytes potentiates vascular damage and permeability in an organoid model of the microvasculature

Khan, Abdullah; Reyat, Jasmeet; Hill, Harriet; Bourne, Joshua; Colicchia, Martina; Newby, Maddy L; Allen, Joel D; Crispin, Max; Youd, Esther; Murray, Paul; Taylor, Graham; Stamataki, Zania; Richter, Alex; Cunningham, Adam; Pugh, Matthew; Rayes, Julie

DOI:

[10.1093/cvr/cvac097](https://doi.org/10.1093/cvr/cvac097)

License:

Creative Commons: Attribution (CC BY)

Document Version

Publisher's PDF, also known as Version of record

Citation for published version (Harvard):

Khan, A, Reyat, J, Hill, H, Bourne, J, Colicchia, M, Newby, ML, Allen, JD, Crispin, M, Youd, E, Murray, P, Taylor, G, Stamataki, Z, Richter, A, Cunningham, A, Pugh, M & Rayes, J 2022, 'Preferential uptake of SARS-CoV-2 by pericytes potentiates vascular damage and permeability in an organoid model of the microvasculature', *Cardiovascular Research*, pp. 1-12. <https://doi.org/10.1093/cvr/cvac097>

[Link to publication on Research at Birmingham portal](#)

General rights

Unless a licence is specified above, all rights (including copyright and moral rights) in this document are retained by the authors and/or the copyright holders. The express permission of the copyright holder must be obtained for any use of this material other than for purposes permitted by law.

- Users may freely distribute the URL that is used to identify this publication.
- Users may download and/or print one copy of the publication from the University of Birmingham research portal for the purpose of private study or non-commercial research.
- User may use extracts from the document in line with the concept of 'fair dealing' under the Copyright, Designs and Patents Act 1988 (?)
- Users may not further distribute the material nor use it for the purposes of commercial gain.

Where a licence is displayed above, please note the terms and conditions of the licence govern your use of this document.

When citing, please reference the published version.

Take down policy

While the University of Birmingham exercises care and attention in making items available there are rare occasions when an item has been uploaded in error or has been deemed to be commercially or otherwise sensitive.

If you believe that this is the case for this document, please contact UBIRA@lists.bham.ac.uk providing details and we will remove access to the work immediately and investigate.

Download date: 02. May. 2024

Preferential uptake of SARS-CoV-2 by pericytes potentiates vascular damage and permeability in an organoid model of the microvasculature

Abdullah O. Khan ^{1*†}, Jasmeet S. Reyat ^{1†}, Harriet Hill ², Joshua H. Bourne ¹, Martina Colicchia ¹, Maddy L. Newby ³, Joel D. Allen³, Max Crispin ³, Esther Youd⁴, Paul G. Murray^{2,5}, Graham Taylor², Zania Stamataki ², Alex G. Richter ², Adam F. Cunningham², Matthew Pugh², and Julie Rayes ^{1*}

¹Institute of Cardiovascular Sciences, College of Medical and Dental Sciences, University of Birmingham, Vincent Drive, Birmingham B15 2TT, UK; ²Institute of Immunology and Immunotherapy, University of Birmingham, Birmingham B15 2TT, UK; ³School of Biological Sciences, University of Southampton, Southampton SO17 1BJ, UK; ⁴Forensic Medicine and Science, University of Glasgow, Glasgow G12 8QQ, UK; and ⁵Health Research Institute, University of Limerick, Limerick V94 T9PX, Ireland

Received 8 October 2021; revised 17 May 2022; accepted 25 May 2022; online publish-ahead-of-print 16 June 2022

Aims

Thrombotic complications and vasculopathy have been extensively associated with severe COVID-19 infection; however, the mechanisms inducing endotheliitis and the disruption of endothelial integrity in the microcirculation are poorly understood. We hypothesized that within the vessel wall, pericytes preferentially take up viral particles and mediate the subsequent loss of vascular integrity.

Methods and results

Immunofluorescence of post-mortem patient sections was used to assess pathophysiological aspects of COVID-19 infection. The effects of COVID-19 on the microvasculature were assessed using a vascular organoid model exposed to live viral particles or recombinant viral antigens. We find increased expression of the viral entry receptor angiotensin-converting enzyme 2 on pericytes when compared to vascular endothelium and a reduction in the expression of the junctional protein CD144, as well as increased cell death, upon treatment with both live virus and/or viral antigens. We observe a dysregulation of genes implicated in vascular permeability, including Notch receptor 3, angiotensin-2, and TEK. Activation of vascular organoids with interleukin-1 β did not have an additive effect on vascular permeability. Spike antigen was detected in some patients' lung pericytes, which was associated with a decrease in CD144 expression and increased platelet recruitment and von Willebrand factor (VWF) deposition in the capillaries of these patients, with thrombi in large vessels rich in VWF and fibrin.

Conclusion

Together, our data indicate that direct viral exposure to the microvasculature modelled by organoid infection and viral antigen treatment results in pericyte infection, detachment, damage, and cell death, disrupting pericyte-endothelial cell crosstalk and increasing microvascular endothelial permeability, which can promote thrombotic and bleeding complications in the microcirculation.

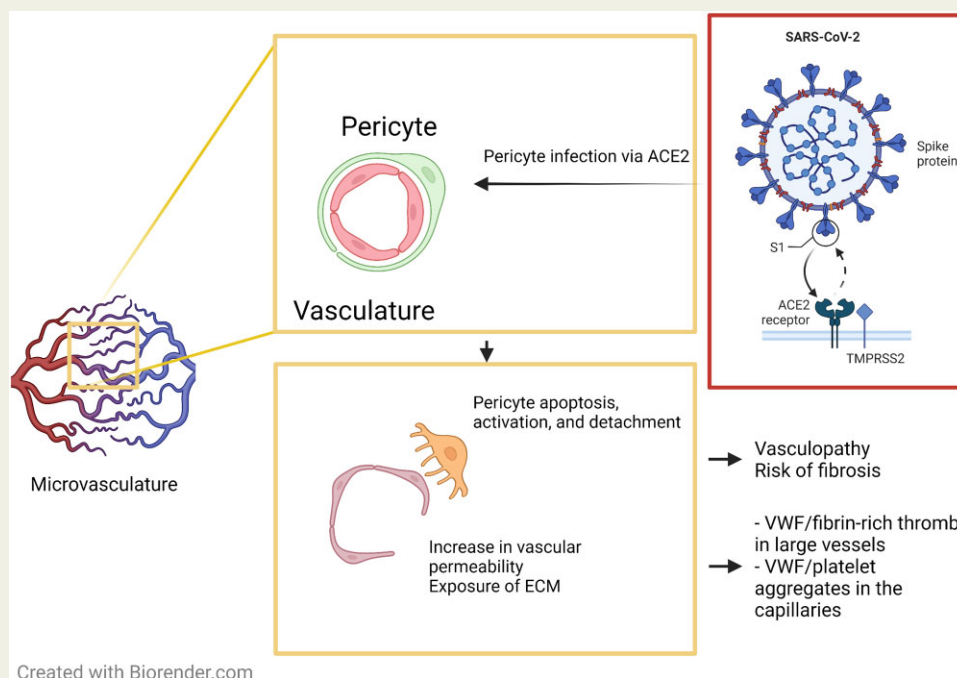
* Corresponding authors. E-mail: j.rayes@bham.ac.uk (J.R.), E-mail: a.khan.4@bham.ac.uk (A.O.K.)

† A.O.K. and J.S.R. have contributed equally.

© The Author(s) 2022. Published by Oxford University Press on behalf of the European Society of Cardiology. All rights reserved.

This is an Open Access article distributed under the terms of the Creative Commons Attribution License (<https://creativecommons.org/licenses/by/4.0/>), which permits unrestricted reuse, distribution, and reproduction in any medium, provided the original work is properly cited.

Graphical Abstract



Pericyte infection by SARS-CoV-2 increases vascular damage and permeability. Preferential uptake of SARS-CoV-2 by pericytes induces their apoptosis leading to the disruption of endothelial cell junctions and the vascular network promoting vascular permeability. SARS-CoV-2-mediated endotheliopathy is associated with thrombotic complications in patients with COVID-19.

Keywords

SARS-CoV-2 • COVID-19 • Endothelial permeability • Thrombosis • Organoids • Vasculopathy

1. Introduction

Severe acute respiratory syndrome coronavirus 2 (SARS-CoV-2)-associated vasculopathy and endotheliitis are commonly observed in patients with severe COVID-19.¹ The incidence of macrovascular thrombosis is relatively high in these patients, with arterial thrombosis and venous thromboembolism observed in over 30% of patients.² Endothelial activation and injury, disruption of cell membrane integrity, intussusceptive angiogenesis, and widespread microthrombi in alveolar capillaries have also been detected in lung autopsies.^{3–5} Under basal conditions, microvascular endothelial cells (ECs) are tightly associated with specialized mural cells (pericytes) that act as integral anchors supporting endothelial vascular integrity and permeability.⁶ Infection and subsequent cell damage induce mural cell activation and apoptosis, driving inflammation and disrupting interactions between pericytes and ECs, increasing vessel instability, vascular permeability, and potentially driving thrombosis and bleeding.⁷ Whether SARS-CoV-2 directly infects ECs and contributes to cell damage and activation remains controversial,^{8,9,10} with increasing evidence supporting key roles for the stroma, as well as innate immune cell and platelet activation in endotheliopathy.^{11,12} Despite the prevalence of these pathologies, the mechanisms driving SARS-CoV-2-mediated endotheliitis and thrombosis both in large vessels and in capillaries remains poorly understood.^{5,13,14}

Following SARS-CoV-2 infection, binding of the viral spike glycoprotein to the host angiotensin-converting enzyme 2 (ACE2) promotes cellular entry, with different proteolytic reactions mediated by transmembrane serine protease 2 (TMPRSS2) and co-receptors required

for efficient virion infection.^{15,16} Infection-mediated disruption of the epithelial barrier allows the virus to infect the vessel wall, with the efficiency of infection being regulated by ACE2 and its co-receptors expression. ACE2 expression on the human endothelium has been shown to be insufficient for viral replication and endothelial activation.⁸ Furthermore, inoculation of primary lung ECs with SARS-CoV-2 results in limited infection rates,^{17,18} while spike pseudovirus can induce mitochondrial damage in ECs.¹⁰ In the absence of clear evidence showing endothelial infection by SARS-CoV-2, other cellular constituents of the vessel wall, such as pericytes, have emerged as potential target cells and sites of infection.^{19–23} Indeed, ACE2 expression on brain and cardiac pericytes has been shown to support SARS-CoV-2 infection.^{22,23} Conversely, lung pericyte infection by SARS-CoV-2 and its effect on EC activation and integrity, in particular, are not well studied.^{20–24} This is at least partially due to the difficulty in modelling pericytes environment *in vitro*, a technical challenge which has been addressed in recent years with the development of organoid models. Indeed, microvascular healthy pericytes express ACE2,^{15,25,26} and this expression can be further increased in pathological conditions such as lung fibrosis,²⁷ a clinical complication observed in patient cohorts known to be vulnerable to COVID-19 infection.²⁸ The ability of SARS-CoV-2 to infect target cells is heavily dependent on the restricted expression of ACE2, TMPRSS2, and novel proteases and cofactors.^{19,26} Using vascular and kidney organoid models, Monteil et al.²⁹ showed that SARS-CoV-2 can directly infect vascular organoids, which can be reversed by human recombinant soluble ACE-2. However, the cell type involved in SARS-CoV-2 uptake and its effect on vessel wall cell activation and survival are not known.

In this study, we assessed the presence of the viral spike glycoprotein in pericytes in lung autopsies from eight patients with COVID-19. We reasoned that direct infection of pericytes with SARS-CoV-2 drives endothelial dysfunction and potentiates thrombotic complications in the microcirculation. We show a heterogeneous presence of the spike glycoprotein in lung microvascular pericytes, in particular, in patients with documented microvascular and macrovascular thrombosis. Infection of 3D vascular organoids mimicking the microvasculature with SARS-CoV-2, spike glycoprotein and nucleocapsid protein-induced pericyte and endothelial death and altered endothelial permeability, independently of endothelial activation. We observed a preferential uptake of SARS-CoV-2 by pericytes associated with a dysregulation of genes regulating endothelial permeability such as Notch receptor 3 (NOTCH3) and angiopoietin-2. Our data suggest that pericytes are a critical site of SARS-CoV-2 infection and disruption of pericyte-endothelial interactions promotes thrombosis.

2. Methods

2.1 Ethical approvals

Collection of post-mortem formalin-fixed paraffin embedded tissue was approved (IRAS: 197937) for tissue obtained via prospective consent post-mortem and retrospective acquisition of tissue in which consent for use in research had already been obtained. Ethics for patient tissue were approved by the Health Research Authority with an National Health Service Research Ethics Committee; approval was issued by North East—Newcastle and North Tyneside 1 (19/NE/0336). All necessary patient/participant written consent has been obtained, and the appropriate institutional forms have been archived. This research adheres to the tenets of the Declaration of Helsinki.

2.2 Patients

Formalin-fixed paraffin embedded lung sections were collected post-mortem from eight COVID-19, one Middle East respiratory syndrome coronavirus (MERS-CoV), one rhinovirus and two control (non-respiratory-associated diseases) patients. COVID-19 samples were from pre-hospital and hospital deceased patients, with time from symptoms to death ranging from 0 to 36 days, and ages ranging from 59 to 89 years old. Patients were not on mechanical ventilation and all had comorbidities (highlighted in [Supplementary material online, Table S1](#)).

2.3 iPSC culture and organoid generation

Human-induced pluripotent stem cells were obtained from Gibco (Thermo) and cultured on GelTrex (Thermo) coated 6-well plates in StemFlex medium (Thermo). Cells were passaged using an ethylenediaminetetraacetic acid dissociation method and routinely karyotyped as described.³⁰ Vascular organoid generation was performed in a manner similar to that previously described.³¹ Briefly, cells were dissociated and replated on Ultra-Low Attachment 6-well plates (Corning) in StemFlex supplemented with RevitaCell (Thermo) overnight before the commencement of differentiation protocol. On Day 0 (d0), cells were collected from Ultra-Low Attachment plates and spun down at 500 g before resuspension in Phase I media, which was comprised of APEL2 (Stem Cell Technologies) media supplemented with CHIR90921 (12 μ M), and BMP4 (Thermo), FGF2, and VEGFA at 50 ng/mL (Stem Cell Technologies). Cells were incubated at 37°C and 5% CO₂ for 3 days, before pelleting by gravitation and resuspension in Phase II medium. Phase II medium was composed of APEL2 medium, VEGFA at 100 ng/mL, and FGF2 at 50 ng/mL. On Day 5

of the protocol, mesodermal blasts were embedded in a mixed matrix hydrogel composed of 60% Collagen Type I (VitroCol—Advanced Biomatrix) and reduced Growth Factor Matrigel (Corning) and incubated in phase II medium supplemented with 15% fetal bovine serum (FBS). Fresh media was added on Day 8, and sprouted cultures were isolated from the hydrogel at Day 10 by scraping and centrifugation. Collected organoids were then cultured individually in 96 well Ultra-Low attachment plates (Corning) before treatment at Day 15.

2.4 Treatment of vascular organoids with SARS-CoV-2 virus or antigens

SARS-CoV-2 England 2 virus (Wuhan) was a kind gift from Christine Bruce, PHE. Recombinant trimeric spike glycoprotein (S) was produced in expressed in human embryonic kidney 293F cells as previously described.³² Nucleocapsid (N) protein was produced in *Escherichia coli* bacteria and purified as described.³³ The levels of endotoxin in the N protein preparation were lower than 0.005 EU/ μ g. Vascular organoids were treated for 48 h with SARS-CoV-2 virus (M.O.I = 0.5) ($n = 3$, 5–15 organoids per experiment). S and N (100 nM) were added to vascular organoids for 72 h in the presence and absence of interleukin (IL)-1 β (20 ng/mL) (Peprotech) ($n = 5$, 5–15 organoids per experiment).

2.5 ELISA

Soluble IL6 (IL6) (Peprotech) and IL8 (Peprotech) were measured in the supernatant of untreated or treated organoids by enzyme-linked immunosorbent assay (ELISA). The levels of von Willebrand factor (VWF) were measured using polyclonal antibodies against VWF (Agilent). Plasma-derived VWF (Wilfactin) was used as a standard.

2.6 Real-time quantitative reverse transcription PCR (qRT-PCR)

Whole organoids were processed using the Micro RNEasy Kit (Qiagen, Germany) according to the manufacturer's instructions. Isolated RNA was quantified on the NanoDrop ND-100 (Thermo Scientific, USA) and cDNA was prepared using 1 μ g RNA using the High Capacity cDNA Reverse Transcription Kit (Applied Biosystems, USA) according to the manufacturer's instructions using standard cycling conditions. cDNA was then diluted to 5 ng before being combined with PowerUp SYBR Green Master Mix reagent (Applied Biosystems) and the relevant pre-designed PrimeTime IDT Primers. The absolute expression of the respective genes was calculated using the Δ Ct method using GAPDH as an internal housekeeping control. Expression values were normalized to control conditions and log-transformed before plotting using GraphPad Prism 7.

2.7 Organoids and lung sections staining

2.7.1 Whole organoid staining

Whole organoids from independent experiments were pooled, fixed for 15 min in PFA 4%, washed in phosphate buffer saline (PBS)-Tween-20 (PBS-T 0.05%) and incubated overnight in blocking buffer [2% goat serum, 1% bovine serum albumin (BSA)] supplemented with Triton- \times 100, and sodium deoxycholate. Samples were then incubated overnight at 4°C in blocking buffer containing primary antibodies (see [Supplementary material online, Table S2](#)). Secondary Alexa Fluor antibodies (all from Invitrogen) were added for 2 h, and washed before staining with 4',6-diamidino-2-phenylindole (DAPI). Upon labelling, samples were washed again in PBS-T, mounted in 0.5% low melting point agarose (Fisher Scientific) in an Ibidi 8-well slide (Ibidi). Samples were then subject to serial dehydration in ethanol (30, 50,

70, 100%) before clearing in ethyl cinnamate and imaging using Airyscan confocal microscopy.

2.7.2 Organoid sections staining

Vascular organoids from independent experiments were fixed for 15 min in PFA 4% and frozen in optimum cutting temperature (OCT) compound (Tissue-Tek, The Netherlands). Sections (12 μ m) were blocked with PBS containing 5% BSA and 10% goat serum for 1 h, and autofluorescence was quenched using ammonium chloride 50 mM for 20 min. Primary antibodies against ACE2 (ThermoFischer scientific) and CD144 (ThermoFischer scientific), Spike glycoprotein (Sinopharma), CD140 b (Sigma-Aldrich), Ulex Europaeus Agglutinin I (UEA1), ACE2 (Thermofisher), and Biotinylated (VECTOR Laboratories) were incubated overnight at 4°C. Click-iT™ terminal deoxynucleotidyl transferase dUTP nick end labeling (TUNEL) Alexa Fluor™ 647 Imaging Assay (ThermoFischer) was used to stain for apoptosis. Secondary antibodies were incubated for 1 h at room temperature. Anti-NG2 Alexa Fluor 488 was incubated for 1 h at RT (see [Supplementary material online, Table S2](#)). Slides are mounted using ProLong Gold Antifade Mountant with DAPI (Life Technologies). Sections were imaged using Epi fluorescent microscopy or Airyscan confocal microscope and analysed using ZEN software and image J.

2.7.3 Lung sections staining

For paraffin sections, following rehydration and antigen retrieval, lung sections were treated with H₂O₂ 3% for 15 min and blocked with PBS containing 5% BSA and 10% goat serum for 1 h. Antibodies against neural/glial antigen 2 (NG2), spike glycoprotein, intercellular adhesion molecule 1, CD144 vascular endothelial-cadherin (VE-cadherin), VWF, platelet CD42b, and fibrin (see [Supplementary material online, Figure S2](#)) were incubated overnight at 4°C. Secondary antibodies were added for 1 h at room temperature. Nuclei were stained using DAPI. Lung autofluorescence was quenched using a commercial kit (Vector laboratories) and slides mounted using ProLong Gold Antifade Mountant (Life Technologies). Sections were imaged using Epi fluorescent microscopy or Zeiss Axio Scan.Z1 microscope and analyzed using ZEN software and image J.

2.8 Flow cytometry

Organoids were harvested and dissociated using 200 U/mL collagenase type-II (Worthington) resuspended in HBSS solution (Sigma-Aldrich). For dissociation, cells were first washed twice with PBS before resuspension in collagenase solution and incubation at 37°C for two 3 min intervals, with brief trituration between each step. The cells were blocked with PBS-FBS 10% for 20 min on ice. Dead/live cells were detected using Live/Dead Fixable Aqua Dead Cell Stain (Thermofischer). Cells were stained with anti-CD144-PEcy7, anti-podoplanin-FITC, anti-CD140 b-PE, anti-CD31-APC-Cy7 (all from Biolegend), anti-intercellular adhesion molecule 1 (ICAM)-1-biotin followed by Streptavidin PE-CF594 (BD), anti-NG2-APC (Bio-Techne Ltd) for 20 min on ice. Cells were fixed and acquired by flow cytometry (Cyan, Beckman Coulter). Cell death is shown as the fraction of cells negative for Live/Dead Fixable Aqua Dead Cell Stain (live cells) over total cells detected within the endothelial fraction (CD31+), fibroblast (CD140b⁺NG2⁻) or pericytes (CD140b⁺NG2⁺) populations. ECs were defined as CD31⁺ and CD144⁺ double-positive cells. The CD140b positive population contained both pericytes (CD140b⁺ NG2⁺) and fibroblasts (CD140b⁺ NG2⁻) as assessed by flow cytometry (see [Supplementary material online, Figure S1](#)). CD144 expression is assessed on CD31⁺ cells (see

[Supplementary material online, Figure S1](#)). Podoplanin and ICAM-1 expression are assessed on pericytes (CD140b⁺ NG2⁺) and fibroblasts (CD140b⁺ NG2⁻).

2.9 Image analysis

Image analysis was performed using Fiji.³⁴ For measures of VE-Cadherin in patient samples, 8–10 images across different slides and sections from each patient were taken and analysed. Within each image, an ROI was drawn around a vessel and the mean intensity of the channel of interest was measured and plotted. For co-localization studies, ROIs were drawn around 5 distinct separate sectioned organoids and the Coloc2 method was applied to find the Pearson's Correlation Co-efficient.

2.10 Data analysis

All data were presented as means \pm standard deviation (s.d.). The significant difference groups were analysed using either a One-Way ANOVA with multiple comparisons or a Kruskal–Wallis Test with multiple comparisons as indicated in figure legends using Prism 7 (GraphPad Software Inc, USA).

3. Results

3.1 Spike glycoprotein is detected in NG2⁺-pericytes in autopsies of patients with COVID-19 and is associated with decreased endothelial permeability and thrombosis

In the presence of conflicting data supporting endothelial viral uptake and with evidence of an emerging role of brain and heart pericytes in SARS-CoV-2 infection,^{19,20} we reasoned that SARS-CoV-2 targets pericytes in the microvasculature of the lung in patients with severe COVID-19, altering the crosstalk with ECs and promoting vascular permeability and damage. As a first step, we assessed the presence of the spike glycoprotein in pericytes of lung tissues obtained post-mortem from eight patients who died from COVID-19 (see [Supplementary material online, Table S1](#)). Immunostaining analysis of the viral spike glycoprotein revealed positive staining in NG2-positive (NG2⁺) pericytes in 5 patients with COVID-19, while it was undetectable in age-matched non-COVID19 control lung autopsies ([Figure 1A–C](#); [Supplementary material online, Figure S2](#)). Notably, the presence of the spike glycoprotein in the lungs and its colocalization with pericytes was heterogenous among patients ([Figure 1B](#); [Supplementary material online, Figure S2](#)). NG2⁺ Spike⁺ cells were not lining the endothelium, in particular, cells with high spike staining (as indicated in [Figure 1B](#)), and Spike signal was associated with ICAM-1 staining ([Figure 1A, C](#)), suggesting pericyte activation and detachment following infection.

Given that microvascular pericyte activation and apoptosis regulate microvascular endothelial permeability,³⁵ we assessed the expression of the endothelial junctional protein VE-cadherin (CD144), as a marker for vascular permeability. In non-ventilated COVID-19 patients, CD144 expression on the microvascular vessels was decreased in SARS-CoV-2 infected lungs compared to control, most markedly in patients with confirmed macro and micro-thrombosis ([Figure 1D and E](#); [Supplementary material online, Figure S3](#)). These results show that spike glycoprotein strongly localizes with lung pericytes and this is associated with increased pericyte detachment and a decrease in endothelial barrier function, in particular in patients with thrombotic complications.

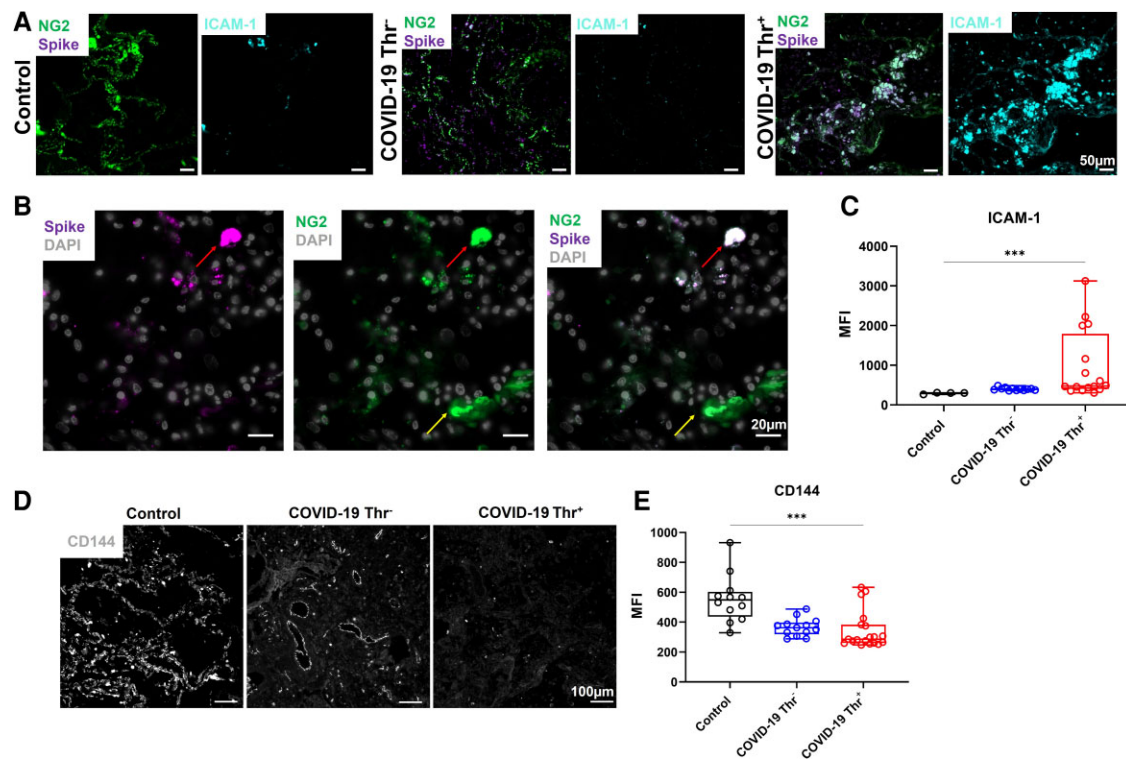


Figure 1 Detection of the spike glycoprotein in lung pericytes and decreased CD144 expression in COVID-19 patients. (A) Immunofluorescence imaging of NG2⁺, spike glycoprotein, and ICAM-1 in formalin-fixed and paraffin-embedded lung from a patient who died from COVID-19 and control COVID-19⁻ (Control) lung sections. (B) High magnification of immunofluorescence imaging of NG2⁺ and spike glycoprotein in lung section. (C) Quantification of ICAM-1 expression using ImageJ in lung autopsies from two patients who died from non-respiratory-associated diseases, four COVID-19 patients without thrombosis and four patients with detectable thrombosis (3–6 areas per slide). (D) Representative immunofluorescence imaging of CD144 (VE-cadherin) in lung sections. (E) Quantification of CD144 levels using ImageJ. One-way ANOVA with multiple comparisons was performed for each statistical test with significance at (*** P < 0.001).

3.2 Increased VWF and fibrin deposition in COVID-19 lungs patients with thrombotic complications

CD144 is crucial for endothelial stability and blockade of CD144 contributes to coagulopathy, particularly in the lung microvasculature.^{36,37} We, therefore, assessed CD144 expression and markers of thrombosis in the lung autopsies of patients with COVID-19. Diffuse alveolar damage with extensive hyaline membrane rich in fibrin was observed in all patients (Figure 2A). Compared to lung autopsies from age-matched controls, we observed a significant decrease in CD144 expression (Figures 1D and E, 2B–D; Supplementary material online, Figure S3) associated with platelet recruitment and VWF deposition in lung capillaries with low fibrin content (Figure 2B–D; Supplementary material online, Figure S4). Thrombi in the large vessels were rich in VWF and fibrin, but with low content in platelets.³⁸ Megakaryocytes (CD42b⁺) were also observed in some patients (Figure 2C). VWF was significantly higher in patients with thrombotic complications, supporting a key role for endothelial activation in thrombosis.

In order to assess whether CD144 downregulation is observed in other coronavirus family member viruses, we also assessed the expression of CD144, platelets (CD42b⁺), and fibrin in lung autopsies from cases of MERS-CoV and rhinovirus. A decrease in CD144 expression

and an increase in fibrin deposition and platelet recruitment in the microvasculature was observed in MERS-CoV-infected lung compared to control lung tissue (Figure 2E), whereas CD144 expression was more evident in the rhinovirus-infected lung without significant fibrin deposition or platelet recruitment (Figure 2F). These results suggest that in this small cohort of patients, a decrease in CD144 expression and an increase in VWF deposition are observed in lung autopsies from patient with COVID-19, in particular with documented thrombosis.

3.3 Preferential SARS-CoV-2 uptake by pericytes in a vascular organoid model

In order to assess the direct role of SARS-CoV-2 on pericytes and ECs, we generated 3D human vascular organoids^{30,31} (Figure 3A) comprised of vascular endothelium (CD144⁺) and pericytes (CD140b⁺) (Figure 3B; Supplementary material online, Figure S1). The percentage of ECs varies between 20 and 50% ECs, 20–50% for NG2⁺CD140b⁺ and 10–40% NG2⁺CD140b⁺. Co-staining of vascular organoid sections with ACE2 and CD144 antibodies indicated a distribution of ACE2 outside the branching junctions of ECs (Figure 3C). ACE2 strongly colocalized with pericytes (NG2⁺, CD140b⁺) with lower colocalization with the endothelial marker UAE1 (Figure 3D–F). Organoids were then exposed to live SARS-CoV-2 virus (M.O.I 0.5) for 48 h, and the distribution

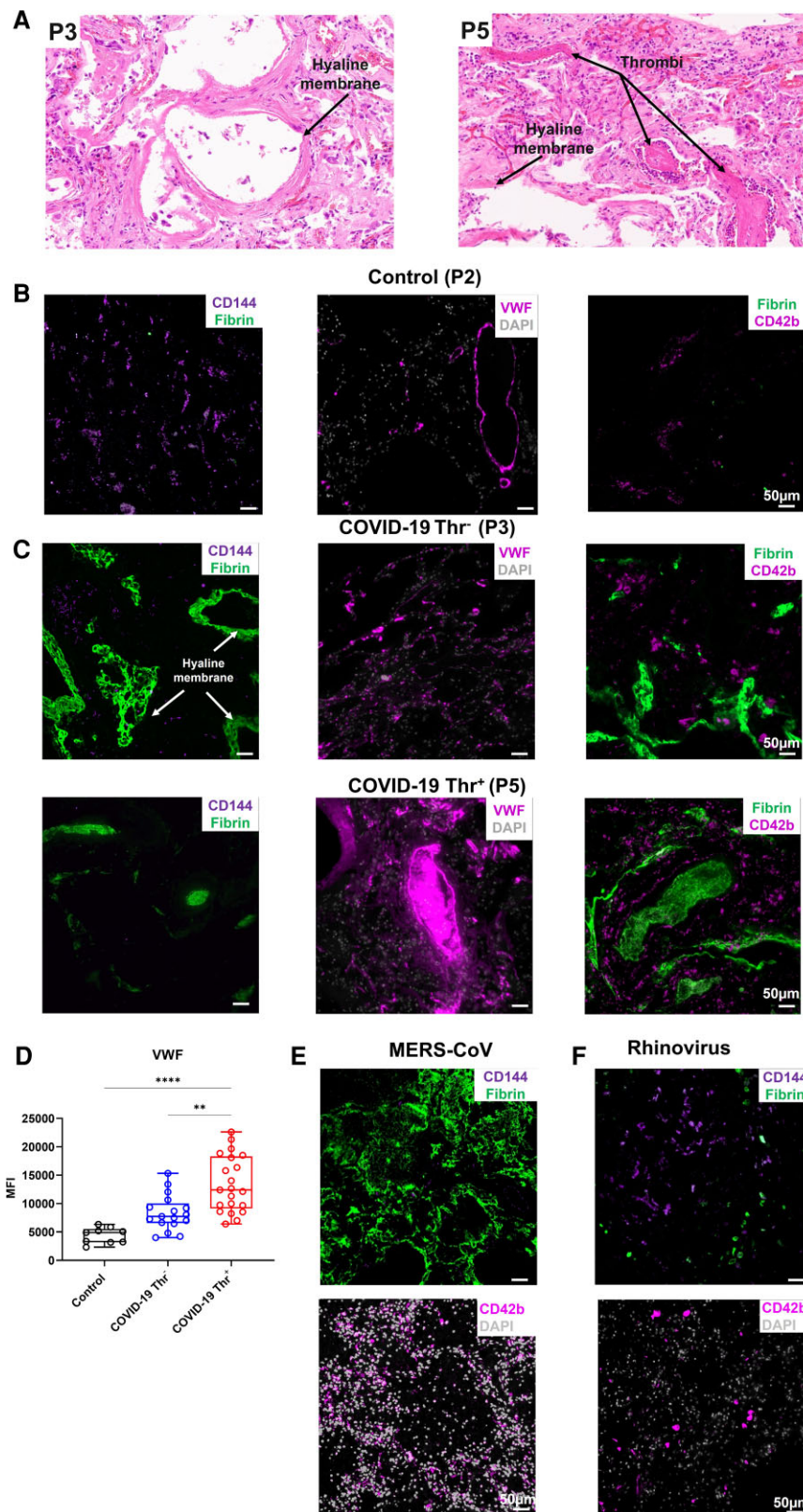


Figure 2 Decreased CD144 expression is associated with increased VWF deposition in the lung of patients with COVID-19. (A) H&E staining of lung sections from patients who died from COVID-19 with or without evidence of thrombosis. (B and C) Immunofluorescence imaging of CD144, VWF, platelets (CD42b), and fibrin in formalin-fixed and paraffin-embedded lung sections. (D) Quantification of VWF in lung sections. (E and F) Staining of CD144, CD42b, fibrin, and DAPI in lung sections from patients infected with (E) MERS-CoV and (F) rhinovirus. Images were captured using a Zeiss Observer 7 Epifluorescence microscope and slide scanner Axio Scan Z1. (Kruskal–Wallis test performed on a total of three to five lung sections from three control patients, three COVID-19 patients with thrombosis, and three without evidences of thrombosis (* $P < 0.05$, ** $P < 0.01$, *** $P < 0.001$, **** $P < 0.0001$).

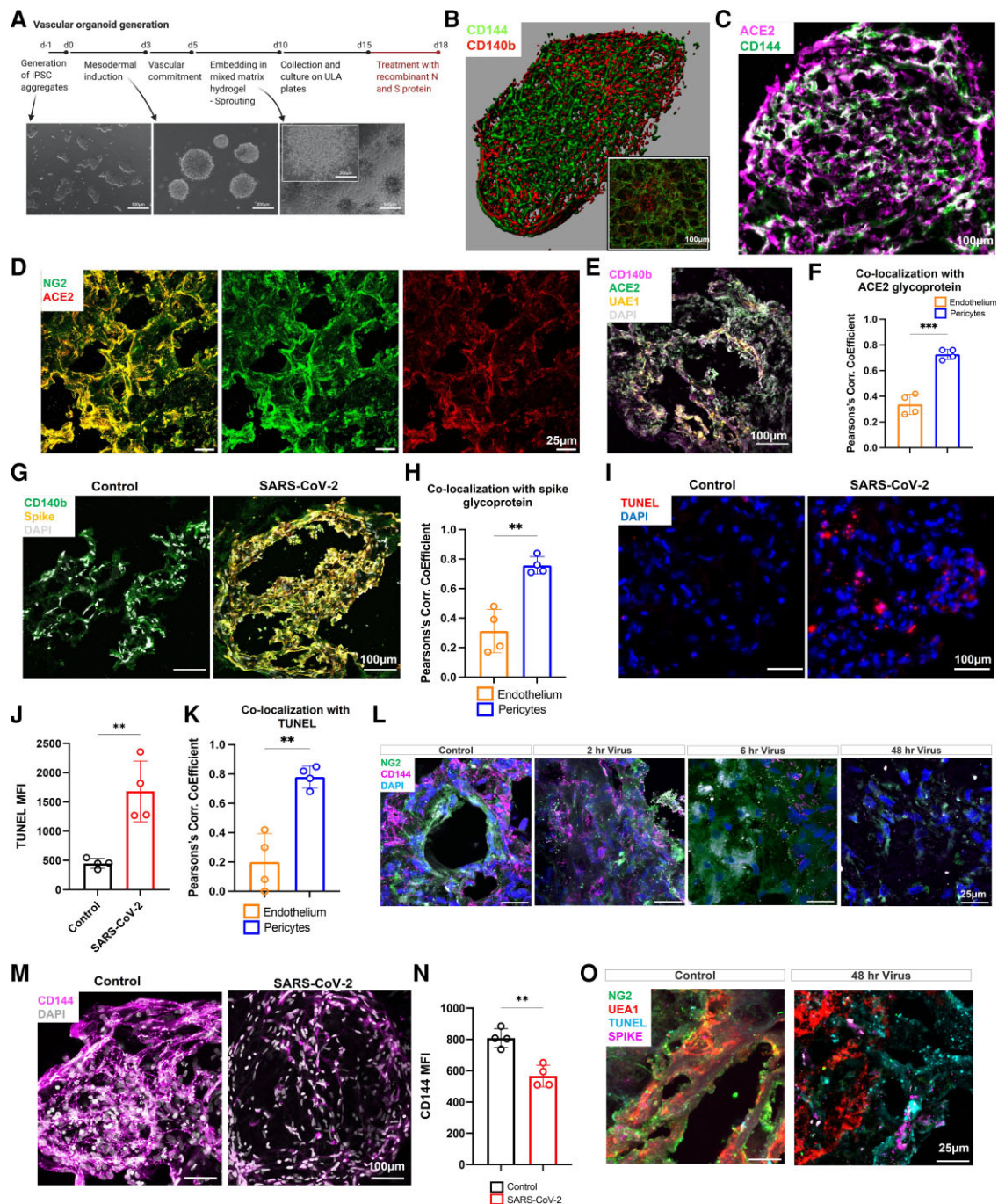


Figure 3 Pericyte preferential uptake of SARS-CoV-2 increases vascular permeability and endothelial and pericyte death in vascular organoids. (A) Vascular organoids were generated using a step-wise differentiation of human-induced pluripotent stem cells. (B) Cell composition and distribution in mature vascular organoids were assessed using immunofluorescence whole-mount microscopy. (C) Immunofluorescence imaging of ACE2 and CD144 positive cells in organoids (12 µm organoid sections). (D) Sections of vascular organoids were co-stained for pericytes (NG2) and ACE2. (E) Staining for UAE-1, ACE2, CD140b, and DAPI in vascular organoids. (F) Co-localization analysis between ACE2 and CD140b compared ACE2 co-localization with UAE1 as measured by the Pearson's correlation coefficient. (G) Co-staining for the spike glycoprotein in endothelial organoids with CD140b⁺ cells treated with SARS-CoV-2. (H) Quantification of co-localization of the spike glycoprotein between endothelium and pericytes. (I) Sections of vascular organoids were stained with apoptosis marker TUNEL and nuclei staining DAPI. (J) Quantification of TUNEL staining in control and SARS-CoV-2 treated vascular organoids. (K) Co-localization of the TUNEL staining with UAE-1 (endothelium) and pericyte (CD140b⁺). (L) Staining of control and SARS-CoV-2-infected organoids for CD144, pericytes (NG2), and nuclei (DAPI). (M) Immunofluorescence imaging of CD144 and nuclei (DAPI) in whole vascular organoids treated with SARS-CoV-2 (M.O.I = 0.5) for 48 h. (N) Quantification of CD144 staining in control and SARS-CoV-2 treated vascular organoids. (O) Staining for NG2, UAE-1, TUNEL, and spike in control and SARS-CoV-2 infected organoids (48 h). N = 4 for organoid experiments, where one replicate is a total of 8–10 individual organoids pooled for assays from each of four independent biological replicates. Each biological repeat was a separate differentiation protocol followed by viral infection. For co-localizations un-paired t-tests were performed (** P = <0.01) Schematic created on Biorender.com.

of the spike glycoprotein was assessed using immunofluorescence imaging (Figure 3G). Colocalization analysis showed a strong presence of the spike in CD140b/NG2⁺ (Figure 3H) with lower levels detected in UAE1-positive ECs (Figure 3I). SARS-CoV-2 infection of vascular organoid was associated with increased cell apoptosis as assessed using TUNEL staining (Figure 3J and E). TUNEL staining was observed in both UAE1-positive ECs and pericytes (CD140b/NG2⁺); however, it was significantly higher in pericytes compared to ECs (Figure 3K). SARS-CoV-2 infection progressively altered the expression and distribution of NG2 within the infected organoids associated with a decrease in CD144 expression (Figure 3L–N). The decrease in CD144 was not due to the loss of ECs as shown using UAE1 staining (see [Supplementary material online, Figure S5](#)). These results show that infection of vascular organoids with SARS-CoV-2 induces pericyte apoptosis and decreases CD144 expression through a preferential uptake of the virus by pericytes. This is associated with a disruption of the vessel architecture, detachment of pericytes and loss of vascular integrity.

3.4 Spike glycoprotein and nucleocapsid protein impair endothelial integrity and survival without significant activation

In order to assess whether the spike glycoprotein is responsible for altered endothelial integrity and cell survival, vascular organoids were treated with (i) recombinant active trimeric spike glycoprotein (S) (100 nM),^{32,39} (ii) nucleocapsid protein (N) (100 nM),³³ or (iii) a combination of both (S + N) for 72 h. Endothelial survival was assessed using live/dead fixable dye staining, while EC activation and permeability were assessed using ICAM-1 and CD144 expression, respectively (see [Supplementary material online, Figure S1](#)). Treatment of vascular organoids with S, N, or S + N decreased EC survival as assessed by a decrease in the fraction of live ECs from total cells (Figure 4A and E). Co-stimulation with IL-1 β , a potent pro-inflammatory cytokine, did not alter cell death compared to viral antigen alone. Similar to SARS-CoV-2 infection, treatment of vascular organoids with viral antigens decreased the number of ECs (CD144⁺/CD31⁺ cells; Figure 4C). Treatment with viral antigens did not induce EC activation as assessed by the expression of ICAM-1 on ECs (Figure 4D). No significant changes in the levels of IL6, IL8, and VWF in the supernatants were observed following viral antigen treatment compared to untreated organoids (Figure 4E–G). These results support a role for N and S protein in regulating EC death and integrity without inducing significant endothelial activation.

3.5 Spike glycoprotein and nucleocapsid protein induce pericyte death in vascular organoids

We further assessed pericyte and fibroblast survival and activation following viral antigen treatment by flow cytometry. Viral antigens N and S decreased pericyte survival as assessed by a decrease in the live fraction of pericytes among total cells (Figure 4H and E). Despite the presence of ICAM-1-positive pericytes in patient lung sections, no significant activation of pericytes was observed in vascular organoids as measured by the expression of ICAM-1 on CD140b⁺NG2⁺ pericytes (Figure 4J). The addition of IL-1 β did not alter cell survival or activation compared to antigen alone (Figure 4J). No significant cell death or activation was observed in the fibroblast population (see [Supplementary material online, Figure S6](#)). These results show that S and N antigens alter pericyte survival without inducing direct activation.

3.6 Spike and N proteins alter gene expression linked to vascular integrity and permeability in vascular organoids

To investigate the mechanisms by which viral infection of the vasculature drives the loss of CD144 expression, we treated vascular organoids with S and N for 4, 24 and 72 h to assess transcriptional changes in key genes involved in the maintenance of vascular barriers by qRT-PCR. These included genes encoding for angiopoietin-1 (ANGPT1), angiopoietin-2 (ANGPT2), sphingosine kinase 1 (SPHK1), sphingosine kinase 2 (SPHK2), NOTCH3, beta-catenin 1 (CTNNB1), Jagged Canonical Notch Ligand 1 (JAG1), Jagged Canonical Notch Ligand 2 (JAG2), CD144 (CDH5), CD31 (PECAM), Tie2 (TEK), ACE2, PDGFRB, Toll-like receptor 4 (TLR4), and Integrin alpha 4 (ITGA4). Compared to untreated organoids, we found significant down-regulation in NOTCH3, SPHK2, and TEK, while in contrast we saw a marked upregulation of ACE2, ANGPT2, and SPHK1 (Figure 3K; [Supplementary material online, Figure S7](#)). No significant changes in CDH5, ANGPT1, or other genes were observed. These results show that S and N treatments alter the expression of gene-regulating vascular integrity and permeability.

4. Discussion

In this study, we used lung autopsy sections from patients with COVID-19 and a 3D vascular organoid model to show that SARS-CoV-2 and its antigens S and N decrease the expression of the adhesion junction molecule CD144 and alter EC and pericyte survival without inducing endothelial activation. We also observe a decrease in CD144 expression in the lung microvasculature of COVID-19 patients that is associated with increased platelet recruitment and VWF deposition. The preferential uptake of SARS-CoV-2 by pericytes in the vascular organoid alters the expression of pericyte and endothelial genes regulating endothelial permeability and integrity, increasing cell permeability and death.

During homeostasis, the integrity of the vasculature is maintained through tight crosstalk between mural and ECs. Pericytes and ECs establish connections to maintain endothelial quiescence through cell–cell contact via ‘Peg-and-socket’ like membrane structures which include tight (claudin, occludin, and JAM-1), gap (connexin43), and adherent (N-cadherin) junctions and through focal adhesion plaques allowing indirect interactions between both cells via the extracellular matrix through integrins.⁴⁰ Pericyte and ECs can also communicate through paracrine signalling of growth factor (angiopoietin-1 and PDGF), their receptors (Tie2 and PDGFRb), and juxtacrine signalling (Jagged1-Notch3).⁶ Following the inflammatory or infectious challenge, as observed during severe SARS-CoV-2 infection, the protective effect of the endothelium is lost, promoting a thrombotic and inflammatory microenvironment, supporting platelet recruitment, activation of the coagulation cascade, and thrombosis. Indeed, endotheliitis, endothelial dysfunction, and death are hallmarks of severe SARS-CoV-2 infection.^{1,41} Using a vascular organoid model, we observed that SARS-CoV-2 or viral antigens S and N downregulate CD144 expression on ECs, increasing cell death. CD144 mediates EC interactions and antibodies blocking this interaction increase endothelial permeability, apoptosis, vascular instability, and hemorrhages.^{42,43} This can also expose the prothrombotic extracellular matrix to blood cells, such as platelets, promoting a thrombotic state.³⁷ The detection of spike glycoprotein in pericytes in vascular organoids and COVID-19 lung autopsies suggests preferential uptake of SARS-CoV-2 by pericytes, probably due to the

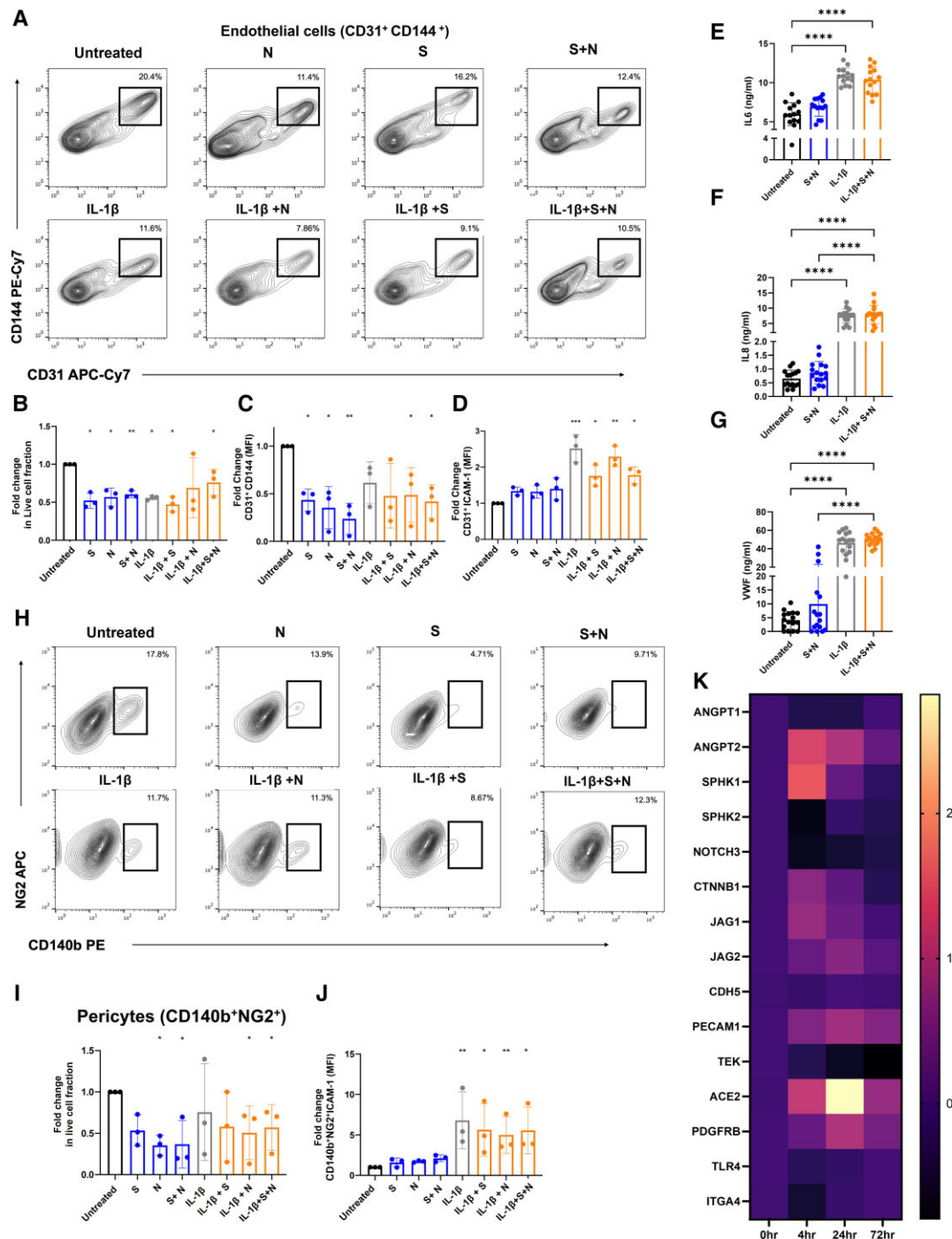


Figure 4 Recombinant viral antigens S and N increase vascular permeability and death without endothelial activation. (A–D) Vascular organoids were treated with spike glycoprotein (S) (100 nM), nucleocapsid (N), or a combination of both proteins for 72 h in the presence or absence of IL-1 β (20 ng/mL) compared to control was measured by flow cytometry. (A) Representative flow cytometry blots of EC treated with S, N, and S+N antigens in the presence and absence of IL-1 β . (B) Fold change in the live population of CD31⁺ cells from the total population using Live/Dead fixable dead cell stain. (C) Fold change in CD144 expression on CD31⁺ cells compared to untreated organoids and (D) fold change in ICAM-1 expression on CD31⁺ cells in treated organoids vs. untreated were measured by flow cytometry. (E) Detection of the levels of soluble IL6, (F) IL8, and (G) VWF in the supernatant of organoids treated for 72 h with viral antigens in the presence or absence of IL-1 β by ELISA ($n = 3$ independent experiments, 3–4 replicate per experiment). (H) Representative flow cytometry plots of pericytes treated with S, N, and S+N antigens in the presence and absence of IL-1 β (20 ng/mL). (I) Live/dead NG2⁺ cells from the total population, (J) fold change in ICAM-1 expression on CD140⁺ NG2⁺ cells in treated organoids vs. untreated were measured by flow cytometry. (K) qPCR of vascular organoids treated with combination S and N proteins for 0, 4, 24, and 72 h for genes regulating endothelial permeability. $N = 3$ for experiments, where one replicate is a total of 12–15 individual organoids pooled for assays from each of three independent biological replicates (independent differentiations). One-way ANOVA with multiple comparisons performed for each statistical test with significance at (* $P < 0.05$, ** $P < 0.01$, *** $P < 0.001$, **** $P < 0.0001$).

high expression of ACE2, is a key contributor for pericyte and endothelial damage.^{44,45} This effect was mediated by pericyte infection, as the presence of the spike glycoprotein was mainly observed in pericytes, both in vascular organoids and COVID-19 lung autopsies. The increase in apoptosis observed could be due to a reduction in the capacity of infected pericytes to support an endothelial network. This, in turn, produces pro-apoptotic factors resulting in EC death as recently shown using primary cardiac pericytes.²² Using a cortical organoid model, pericytes were shown to serve as a replication site for SARS-CoV-2 allowing viral production, transport, and infection of other cells such as astrocytes mediating their death.²³ In a model of vascular organoids, SARS-CoV-2 infection and replication were inhibited by human soluble recombinant ACE2, although the cell type involved was not identified.²⁹ In this study, we identified the pericytes as the main cells responsible for SARS-CoV-2 uptake within the vascular organoids. SARS-CoV-2 infection of pericytes in vascular organoids results in increased apoptosis in both pericytes and ECs, thereby increasing vascular permeability. Moreover, the loss of pericytes increases EC sprouting and intussusceptive angiogenesis in SARS-CoV-2-infected lungs combined with disruption of intercellular junctions, cell swelling and a loss of contact with the basal membrane.⁵ Despite a lower expression of ACE2 on ECs, SARS-CoV-2 can also directly impair endothelial permeability by acting directly on ECs.⁴⁶ The effect of spike protein-mediated endothelial dysfunction was further increased on diabetic ECs, supporting a role for chronic disease-induced vessel damage in the high susceptibility to cell damage. The effect of the spike is not limited to CD144, as a significant decrease in the tight junction protein JAM-A and the gap junction protein connexin-43 were also observed.⁴⁶ We did not observe an alteration in the gene expression of CDH5, suggesting CD144 undergoes internalization and degradation. Indeed, it was recently shown that the spike protein-induced internalization of ACE2 triggered the subsequent internalization and degradation of key junction proteins impairing endothelial barrier integrity.⁴⁵

In addition to the decrease in endothelial junction protein CD144, we observed that addition of the spike and N proteins induced gene expression of angiotensin-2 while downregulating NOTCH3. These data are consistent with previous observations showing that knockdown of NOTCH3 using siRNA increases proinflammatory genes, including angiotensin-2 and ICAM-1, induces pericyte dysfunction and pericyte-EC interaction destabilization promoting vascular leakage. Angiotensin-2 is a non-signal transducing ligand of Tie-2 produced by ECs. Activation of the Tie-2 signalling pathway by angiotensin-2 destabilizing the vasculature by inhibiting the protecting effect of angiotensin-1. Moreover, angiotensin-2 induces pericyte damage and detachment, increasing vascular leakage and immune cell migration. This process increases plasminogen activator inhibitor-1 (PAI-1) in ECs, which supports coagulation, endothelial activation, and inflammation.⁴⁷ An increase in the levels of angiotensin-2⁴⁸ and PAI-1⁴⁹ is observed in patients with COVID-19 and associates with thrombo-embolic events.

Pericyte activation and dysfunction increase EC procoagulant activity and endothelial permeability, as constitutive hypoplasia of pericytes increases VWF release, tissue factor expression, and platelet adhesion. In this study, we did not observe a significant increase in VWF in the supernatant of vascular organoids treated with viral antigens, suggesting that VWF release associated with endothelial activation may result from the dysregulated immune/inflammatory response associated with SARS-CoV-2 infection rather than pericyte or EC infection.^{50–54} With the lack of efficacy of anti-platelet drugs in improving outcome in severe

COVID-19 patients^{38,55,56} endothelial activation and release of VWF represents a potential target to limit thrombosis in COVID-19 patients. Recently, platelet activation and secretion of S100 A8/A9, a damage-associated molecular pattern, was shown to induce endothelial activation, supporting a role for platelet recruitment and activation in endotheliitis.¹¹ These effects can be exacerbated by comorbidities, which can increase endothelial and pericyte responses to infection. Further studies using vascular organoid models mimicking disease state can shed light on the mechanisms of endothelial activation during SARS-CoV-2 infection.

Our study has, however, some limitations. The detection of spike glycoprotein in lung pericytes was heterogenous in our small cohort of lung autopsies. This could be due to different infection rate and incubation time, patients' comorbidities, or other unknown factors. The infection of pericytes was shown using our vascular organoid model as well as a cortical organoid model, supporting a key role for pericyte infection in altering the communication with neighbouring cells. Moreover, these observations need to be validated in a larger number of lung autopsies, due to the limited sections available for this study.

In conclusion, we propose that direct infection of pericytes by SARS-CoV-2 induces pericyte damage and dysregulates the crosstalk with ECs, increasing vascular permeability. However, endothelial activation is more likely regulated by the inflammatory response and platelet recruitment and activation, in particular, in the microcirculation rather than direct viral infection and combined endothelial activation and increased vascular permeability promotes vasculopathies.

Supplementary material

Supplementary material is available at *Cardiovascular Research* online.

Authors' contributions

A.O.K. and J.R. designed research, performed research, analysed data and wrote the paper; J.S.R. performed research and analysed data; J.H.B. and M.C. contributed to data analysis; M.L.N., J.D.A., M.C., A.F. contributed vital new reagents; E.Y., P.G.M., G.T., A.G.R. contributes to clinical information and samples collection; Z.S., H.H. and M.P. contributed vital new reagents, performed experiments and analysed data; All authors read and approved the paper.

Acknowledgements

A.O.K. is a Henry Wellcome fellow (218649/Z/19/Z). J.R. is a British Heart Foundation Intermediate Fellow (FS/IBSRF/20/25039). This research was supported by BHF Accelerator Awards to J.S.R. and A.O.K. (AA/18/2/34218). This research was funded, in whole or in part, by the Wellcome Trust (218649/Z/19/Z), British Heart Foundation (AA/18/2/34218), and COMPARE. A CC BY or equivalent licence is applied to AAM arising from this submission, in accordance with the grant's open access conditions. M.C. was supported by the University of Southampton Coronavirus Response Fund. M.C. was also supported by the International AIDS Vaccine Initiative (IAVI) through grant INV-008352/OPP1153692 and the IAVI Neutralizing Antibody Center through the Collaboration for AIDS Vaccine Discovery grant INV-008813/OPP1196345, both funded by the Bill and Melinda Gates Foundation.

Conflict of interest: none declared.

Data availability

Any relevant data is available on request.

References

- Varga Z, Flammer AJ, Steiger P, Haberecker M, Andermatt R, Zinkernagel AS, Mehra MR, Schuepbach RA, Ruschitzka F, Moch H. Endothelial cell infection and endothelitis in COVID-19. *Lancet* 2020;**395**:1417–1418.
- Klok FA, Kruip M, van der Meer NJM, Arbous MS, Gommers D, Kant KM, Kaptein FHJ, van Paassen J, Stals MAM, Huisman MV, Endeman H. Incidence of thrombotic complications in critically ill ICU patients with COVID-19. *Thromb Res* 2020;**191**:145–147.
- Rapkiewicz AV, Mai X, Carsons SE, Pittaluga S, Kleiner DE, Berger JS, Thomas S, Adler NM, Charytan DM, Gasmi B, Hochman JS, Reynolds HR. Megakaryocytes and platelet-fibrin thrombi characterize multi-organ thrombosis at autopsy in COVID-19: a case series. *EClinicalMedicine* 2020;**24**:100434.
- Wichmann D, Sperhake JP, Lutgehetmann M, Steurer S, Edler C, Heinemann A, Heinrich F, Mushumba H, Kniep I, Schröder AS, Burdelski C, de Heer G, Nierhaus A, Frings D, Pfefferle S, Becker H, Bredereke-Wiedling H, de Weerth A, Paschen HR, Sheikhzadeh-Eggers S, Stang A, Schmiedel S, Bokemeyer C, Addo MM, Aepfelbacher M, Puschel K, Kluge S. Autopsy findings and venous thromboembolism in patients with COVID-19: a prospective cohort study. *Ann Intern Med* 2020;**173**:268–277.
- Ackermann M, Mentzer SJ, Jonigk D. Pulmonary vascular pathology in Covid-19. Reply. *N Engl J Med* 2020;**383**:888–889.
- Armulik A, Abramsson A, Betsholtz C. Endothelial/pericyte interactions. *Circ Res* 2005;**97**:512–523.
- Rayes J, Jadoui S, Lax S, Gros A, Wichaiyo S, Ollivier V, Denis CV, Ware J, Nieswandt B, Jandrot-Perrus M, Watson SP, Ho-Tin-Noe B. The contribution of platelet glycoprotein receptors to inflammatory bleeding prevention is stimulus and organ dependent. *Haematologica* 2018;**103**:e256–e258.
- McCracken IR, Saginc G, He L, Huseynov A, Daniels A, Fletcher S, Peghaire C, Kalna V, Andaloussi-Mae M, Muhl L, Craig NM, Griffiths SJ, Haas JG, Tait-Burkard C, Lendahl U, Birdsey GM, Betsholtz C, Nosedo M, Baker AH, Randi AM. Lack of evidence of angiotensin-converting enzyme 2 expression and replicative infection by SARS-CoV-2 in human endothelial cells. *Circulation* 2021;**143**:865–868.
- Qian Y, Lei T, Patel PS, Lee CH, Monaghan-Nichols P, Xin HB, Qiu J, Fu M. Direct activation of endothelial cells by SARS-CoV-2 nucleocapsid protein is blocked by Simvastatin. *J Virol* 2021;**95**(23):e0139621.
- Lei Y, Zhang J, Schiavon CR, He M, Chen L, Shen H, Zhang Y, Yin Q, Cho Y, Andrade L, Shadel GS, Hepokoski M, Lei T, Wang H, Zhang J, Yuan JX, Malhotra A, Manor U, Wang S, Yuan ZY, Shyy JY. SARS-CoV-2 spike protein impairs endothelial function via downregulation of ACE 2. *Circ Res* 2021;**128**:1323–1326.
- Barrett TJ, Cornwell M, Myndzar K, Rolling CC, Xia Y, Drenkova K, Biebuyck A, Fields AT, Tawil M, Luttrell-Williams E, Yuriditsky E, Smith G, Cotzia P, Neal MD, Kornblith LZ, Pittaluga S, Rapkiewicz AV, Burgess HM, Mohr I, Stapleford KA, Voora D, Ruggles K, Hochman J, Berger JS. Platelets amplify endotheliopathy in COVID-19. *Sci Adv* 2021;**7**:eab4234.
- Hottz ED, Azevedo-Quintanilha IG, Palhinha L, Teixeira L, Barreto EA, Pao CRR, Rigby C, Franco S, Souza TML, Kurtz P, Bozza FA, Bozza PT. Platelet activation and platelet-monocyte aggregate formation trigger tissue factor expression in patients with severe COVID-19. *Blood* 2020;**136**:1330–1341.
- Connors JM, Levy JH. COVID-19 and its implications for thrombosis and anticoagulation. *Blood* 2020;**135**:2033–2040.
- Borczuk AC, Salvatore SP, Seshan SV, Patel SS, Bussell JB, Mostyka M, Elsoukary S, He B, Del Vecchio C, Fortarezza F, Pezzuto F, Navales P, Crisanti A, Fowkes ME, Bryce CH, Calabrese F, Beasley MB. COVID-19 pulmonary pathology: a multi-institutional autopsy cohort from Italy and New York City. *Mod Pathol* 2020;**33**:2156–2168.
- Muus C, Lueken MD, Eraslan G, Sikkema L, Waghay A, Heimberg G, Kobayashi Y, Vaishnav ED, Subramanian A, Smillie C, Jagadeesh KA, Duong ET, Fiskin E, Triglia ET, Ansari M, Cai P, Lin B, Buchanan J, Chen S, Shu J, Haber AL, Chung H, Montoro DT, Adams T, Aliee H, Allon SJ, Andrusivova Z, Angelidis I, Ashenberg O, Bassler K, Becavin C, Benhar I, Bergenstrahle J, Bergenstrahle L, Bolt L, Braun E, Bui LT, Callori S, Chaffin M, Chichelnitskiy E, Chiou J, Conlon TM, Cuoco MS, Cuomo ASE, Deprez M, Duclos G, Fine D, Fischer DS, Ghazanfar S, Gillich A, Giotti B, Gould J, Guo M, Gutierrez AJ, Habermann AC, Harvey T, He P, Hou X, Hu L, Hu Y, Jaiswal A, Ji L, Jiang P, Kapellos TS, Kuo CS, Larsson L, Leney-Greene MA, Lim K, Litvinukova M, Ludwig LS, Lukassen S, Luo W, Maatz H, Madisooson E, Mamanova L, Manakongtreecheep K, Leroy S, Mayr CH, Mbano IM, McAdams AM, Nabhan AN, Nyquist SK, Penland L, Poirion OB, Poli S, Qi C, Queen R, Reichard D, Rosas I, Schupp JC, Shea CV, Shi X, Sinha R, Sit RV, Slowikowski K, Slyper M, Smith NP, Sountoulidis A, Strunz M, Sullivan TB, Sun D, Talavera-Lopez C, Tan P, Tantivit J, Travaglini KJ, Tucker NR, Vernon KA, Wadsworth MH, Waldman J, Wang X, Xu K, Yan W, Zhao W, Ziegler CGK, NHLBI LungMap Consortium, Human Cell Atlas Lung Biological Network. Single-cell meta-analysis of SARS-CoV-2 entry genes across tissues and demographics. *Nat Med* 2021;**27**:546–559.
- Clausen TM, Sandoval DR, Spliid CB, Pihl J, Perrett HR, Painter CD, Narayanan A, Majowicz SA, Kwong EM, McVicar RN, Thacker BE, Glass CA, Yang Z, Torres JL, Golden GJ, Bartels PL, Porrell RN, Garretson AF, Laubach L, Feldman J, Yin X, Pu Y, Hauser BM, Caradonna TM, Kellman BP, Martino C, Gordts P, Chanda SK, Schmidt AG, Godula K, Leibel SL, Jose J, Corbett KD, Ward AB, Carlin AF, Esko JD. SARS-CoV-2 infection depends on cellular heparan sulfate and ACE2. *Cell* 2020;**183**:1043–1057.e15.
- Hou YJ, Okuda K, Edwards CE, Martinez DR, Asakura T, Dinno KH III, Kato T, Lee RE, Yount BL, Mascenik TM, Chen G, Olivier KN, Ghio A, Tse LV, Leist SR, Gralinski LE, Schafer A, Dang H, Gilmore R, Nakano S, Sun L, Fulcher ML, Livraghi-Buttrico A, Nicely NI, Cameron M, Cameron C, Kelvin DJ, de Silva A, Margolis DM, Markmann A, Bartelt L, Zumwalt R, Martinez FJ, Salvatore SP, Borczuk A, Tata PR, Sontake V, Kimple A, Jaspers I, O'Neal WK, Randell SH, Boucher RC, Baric RS. SARS-CoV-2 reverse genetics reveals a variable infection gradient in the respiratory tract. *Cell* 2020;**182**:429–446.e414.
- Bernard I, Limonta D, Mahal LK, Hobman TC. Endothelium infection and dysregulation by SARS-CoV-2: evidence and caveats in COVID-19. *Viruses* 2020;**13**:29.
- Chen R, Wang K, Yu J, Howard D, French L, Chen Z, Wen C, Xu Z. The spatial and cell-type distribution of SARS-CoV-2 receptor ACE2 in the human and mouse brains. *Front Neurol* 2020;**11**:573095.
- Chen L, Li X, Chen M, Feng Y, Xiong C. The ACE2 expression in human heart indicates new potential mechanism of heart injury among patients infected with SARS-CoV-2. *Cardiovasc Res* 2020;**116**:1097–1100.
- Wong DWL, Klinkhammer BM, Djurdjaj S, Villwock S, Timm MC, Buhl EM, Wucherpfennig S, Cacchi C, Braunschweig T, Knuchel-Clarke R, Jonigk D, Werlein C, Bulow RD, Dahl E, von Stillfried S, Boor P. Multisystemic cellular tropism of SARS-CoV-2 in autopsies of COVID-19 patients. *Cells* 2021;**10**:1900.
- Avolio E, Carrabba M, Milligan R, Kavanagh Williamson M, Beltrami AP, Gupta K, Elvers KT, Gamez M, Foster RR, Gillespie K, Hamilton F, Arnold D, Berger I, Davidson AD, Hill D, Caputo M, Madeddu P. The SARS-CoV-2 spike protein disrupts human cardiac pericytes function through CD147 receptor-mediated signalling: a potential non-infective mechanism of COVID-19 microvascular disease. *Clin Sci (Lond)* 2021;**135**:2667–2689.
- Wang L, Sievert D, Clark AE, Lee S, Federman H, Gastfriend BD, Shusta EV, Palecek SP, Carlin AF, Gleeson JG. A human three-dimensional neural-perivascular 'assembloid' promotes astrocytic development and enables modeling of SARS-CoV-2 neuropathology. *Nat Med* 2021;**27**:1600–1606.
- Stark K, Eckart A, Haidari S, Tirniceru A, Lorenz M, von Bruhl ML, Gartner F, Khandoga AG, Legate KR, Pless R, Hepper I, Lauber K, Walzog B, Massberg S. Capillary and arteriolar pericytes attract innate leukocytes exiting through venules and 'instruct' them with pattern-recognition and motility programs. *Nat Immunol* 2013;**14**:41–51.
- Teuwen LA, Geldhof V, Pasut A, Carmeliet P. COVID-19: the vasculature unleashed. *Nat Rev Immunol* 2020;**20**:389–391.
- Delorey TM, Ziegler CGK, Heimberg G, Normand R, Yang Y, Segerstolpe A, Abbondanza D, Fleming SJ, Subramanian A, Montoro DT, Jagadeesh KA, Dey KK, Sen P, Slyper M, Pita-Juarez YH, Phillips D, Bloom-Ackerman Z, Barkas N, Ganna A, Gomez J, Normandin E, Naderi P, Popov YV, Raju SS, Niezen S, Tsai LT, Siddle KJ, Sud M, Tran VM, Vellarikkal SK, Amir-Zilberstein L, Atri DS, Beecham J, Brook OR, Chen J, Divakar P, Dorceus P, Engreitz JM, Essene A, Fitzgerald DM, Fropf R, Gazal S, Gould J, Grzyb J, Harvey T, Hecht J, Hether T, Jane-Valbuena J, Leney-Greene M, Ma H, McCabe C, McLoughlin DE, Miller EM, Muus C, Niemi M, Padera R, Pan L, Pant D, Pe'er C, Pfiffner-Borges J, Pinto CJ, Plaisted J, Reeves J, Ross M, Rudy M, Rueckert EH, Siciliano M, Sturm A, Todres E, Waghay A, Warren S, Zhang S, Zollinger DR, Cosimi L, Gupta RM, Hacohen N, Hide W, Price AL, Rajagopal J, Tata PR, Riedel S, Szabo G, Tickle TL, Hung D, Sabeti PC, Novak R, Rogers R, Ingber DE, Gordon Jiang Z, Juric D, Babadi M, Farhi SL, Stone JR, Vlachos IS, Solomon IH, Ashenberg O, Porter CBM, Li B, Shalek AK, Villani AC, Rozenblatt-Rosen O, Regev A. A single-cell and spatial atlas of autopsy tissues reveals pathology and cellular targets of SARS-CoV-2. *bioRxiv* 2021.
- Guo J, Wei X, Li Q, Li L, Yang Z, Shi Y, Qin Y, Zhang X, Wang X, Zhi X, Meng D. Single-cell RNA analysis on ACE2 expression provides insights into SARS-CoV-2 potential entry into the bloodstream and heart injury. *J Cell Physiol* 2020;**235**:9884–9894.
- Meiners S, Eickelberg O, Konigshoff M. Hallmarks of the ageing lung. *Eur Respir J* 2015;**45**:807–827.
- Monteil V, Kwon H, Prado P, Hagelkruys A, Wimmer RA, Stahl M, Leopoldi A, Garreta E, Hurtado Del Pozo C, Prosper F, Romero JP, Wirnsberger G, Zhang H, Slutsky AS, Conder R, Montserrat N, Mirazimi A, Penninger JM. Inhibition of SARS-CoV-2 infections in engineered human tissues using clinical-grade soluble human ACE2. *Cell* 2020;**181**:905–913.e907.
- Khan AO, Slater A, MacLachlan A, Nicolson PLR, Pike JA, Reyat JS, Yule J, Stapley R, Rayes J, Thomas SG, Morgan NV. Post-translational polymodification of beta1-tubulin regulates motor protein localisation in platelet production and function. *Haematologica* 2022;**107**(1):243–259.
- Wimmer RA, Leopoldi A, Aichinger M, Kerjaschki D, Penninger JM. Generation of blood vessel organoids from human pluripotent stem cells. *Nat Protoc* 2019;**14**:3082–3100.
- Watanabe Y, Allen JD, Wrapp D, McLellan JS, Crispin M. Site-specific glycan analysis of the SARS-CoV-2 spike. *Science* 2020;**369**:330–333.
- Faustini SE, Jossi SE, Perez-Toledo M, Shields A, Allen JD, Watanabe Y, Newby ML, Cook A, Willcox CR, Salim M, Goodall M, Heaney JL, Marcial-Juarez E, Morley GL, Torlinska B, Wraith DC, Veenith T, Harding S, Jolles S, Mark PJ, Plant T, Huissoon A, O'Shea MK, Willcox BE, Drayson MT, Crispin M, Cunningham AF, Richter AG. Detection of antibodies to the SARS-CoV-2 spike glycoprotein in both serum and saliva enhances detection of infection. *medRxiv* 2020.

34. Schindelin J, Arganda-Carreras I, Frise E, Kaynig V, Longair M, Pietzsch T, Preibisch S, Rueden C, Saalfeld S, Schmid B, Tinevez JY, White DJ, Hartenstein V, Eliceiri K, Tomancak P, Cardona A. Fiji: an open-source platform for biological-image analysis. *Nat Methods* 2012;**9**:676–682.
35. Kato K, Dieguez-Hurtado R, Park DY, Hong SP, Kato-Azuma S, Adams S, Stehling M, Trappmann B, Wraha JL, Koh GY, Adams RH. Pulmonary pericytes regulate lung morphogenesis. *Nat Commun* 2018; **9**:2448.
36. Duong CN, Nottebaum AF, Butz S, Volkery S, Zeuschner D, Stehling M, Vestweber D. Interference with ESAM (endothelial cell-selective adhesion molecule) plus vascular endothelial-cadherin causes immediate lethality and lung-specific blood coagulation. *Arterioscler Thromb Vasc Biol* 2020;**40**:378–393.
37. Corada M, Mariotti M, Thurston G, Smith K, Kunkel R, Brockhaus M, Lampugnani MG, Martin-Padura I, Stoppacciaro A, Ruco L, McDonald DM, Ward PA, Dejana E. Vascular endothelial-cadherin is an important determinant of microvascular integrity in vivo. *Proc Natl Acad Sci U S A* 1999;**96**:9815–9820.
38. Schrottmaier WC, Pirabe A, Pereyra D, Heber S, Hackl H, Schmuckenschlager A, Brunnthaler L, Santol J, Kammerer K, Oosterlee J, Pawelka E, Treiber SM, Khan AO, Pugh M, Traugott MT, Schorrenhofer C, Seitz T, Karolyi M, Jilma B, Rayes J, Zoufaly A, Assinger A. Adverse outcome in COVID-19 is associated with an aggravating hypo-responsive platelet phenotype. *Front Cardiovasc Med* 2021;**8**:795624.
39. Hsieh CL, Goldsmith JA, Schaub JM, DiVenere AM, Kuo HC, Javanmardi K, Le KC, Wrapp D, Lee AG, Liu Y, Chou CW, Byrne PO, Hjorth CK, Johnson NV, Ludes-Meyers J, Nguyen AW, Park J, Wang N, Amengor D, Lavinder JJ, Ippolito GC, Maynard JA, Finkelstein J, McLellan JS. Structure-based design of prefusion-stabilized SARS-CoV-2 spikes. *Science* 2020;**369**:1501–1505.
40. Duong CN, Vestweber D. Mechanisms ensuring endothelial junction integrity beyond VE-cadherin. *Front Physiol* 2020;**11**:519.
41. Jin Y, Ji W, Yang H, Chen S, Zhang W, Duan G. Endothelial activation and dysfunction in COVID-19: from basic mechanisms to potential therapeutic approaches. *Signal Transduct Target Ther* 2020;**5**:293.
42. Corada M, Liao F, Lindgren M, Lampugnani MG, Breviario F, Frank R, Muller WA, Hicklin DJ, Bohlen P, Dejana E. Monoclonal antibodies directed to different regions of vascular endothelial cadherin extracellular domain affect adhesion and clustering of the protein and modulate endothelial permeability. *Blood* 2001;**97**:1679–1684.
43. Dejana E, Orsenigo F, Lampugnani MG. The role of adherens junctions and VE-cadherin in the control of vascular permeability. *J Cell Sci* 2008;**121**:2115–2122.
44. Cardot-Leccia N, Hubiche T, Dellamonica J, Burel-Vandenbos F, Passeron T. Pericyte alteration sheds light on micro-vasculopathy in COVID-19 infection. *Intensive Care Med* 2020;**46**:1777–1778.
45. Raghavan S, Kenchappa DB, Leo MD. SARS-CoV-2 spike protein induces degradation of junctional proteins that maintain endothelial barrier integrity. *Front Cardiovasc Med* 2021; **8**:687783.
46. Rauti R, Shahoha M, Leichtmann-Bardoogo Y, Nasser R, Paz E, Tamir R, Miller V, Babich T, Shaked K, Ehrlich A, Ioannidis K, Nahmias Y, Sharan R, Ashery U, Maoz BM. Effect of SARS-CoV-2 proteins on vascular permeability. *Elife* 2021;**10**:e69314.
47. Akwii RG, Sajib MS, Zahra FT, Mikelis CM. Role of angiotensin-2 in vascular physiology and pathophysiology. *Cells* 2019;**8**:471.
48. Smadja DM, Guerin CL, Chocron R, Yatim N, Boussier J, Gendron N, Khider L, Hadjadj J, Goudot G, Debuc B, Juvin P, Hauw-Berlemont C, Augy JL, Peron N, Messas E, Planquette B, Sanchez O, Charbit B, Gaussem P, Duffy D, Terrier B, Mirault T, Diehl JL. Angiotensin-2 as a marker of endothelial activation is a good predictor factor for intensive care unit admission of COVID-19 patients. *Angiogenesis* 2020;**23**:611–620.
49. Zuo Y, Warnock M, Harbaugh A, Yalavarthi S, Gockman K, Zuo M, Madison JA, Knight JS, Kanthi Y, Lawrence DA. Plasma tissue plasminogen activator and plasminogen activator inhibitor-1 in hospitalized COVID-19 patients. *Sci Rep* 2021;**11**:1580.
50. Rauch A, Dupont A, Goutay J, Caplan M, Staessens S, Moussa M, Jeanpierre E, Corseaux D, Lefevre G, Lassalle F, Faure K, Lambert M, Duhamel A, Labreuche J, Garrigue D, De Meyer SF, Staels B, Van Belle E, Vincent F, Kipnis E, Lenting PJ, Poissy J, Susen S, Lille COVID Research Network (LICORNE), Members of the LICORNE Scientific Committee. Endotheliopathy is induced by plasma from critically ill patients and associated with organ failure in severe COVID-19. *Circulation* 2020;**142**:1881–1884.
51. Goshua G, Pine AB, Meizlish ML, Chang CH, Zhang H, Bahel P, Baluza A, Bar N, Bona RD, Burns AJ, Dela Cruz CS, Dumont A, Halene S, Hwa J, Koff J, Menninger H, Neparidze N, Price C, Siner JM, Tormey C, Rinder HM, Chun HJ, Lee AL. Endotheliopathy in COVID-19-associated coagulopathy: evidence from a single-centre, cross-sectional study. *Lancet Haematol* 2020;**7**:e575–e582.
52. Philippe A, Chocron R, Gendron N, Bory O, Beauvais A, Peron N, Khider L, Guerin CL, Goudot G, Levasseur F, Peronino C, Duchemin J, Brichet J, Sourdeau E, Desvard F, Bertil S, Pene F, Cheurfa C, Szebel TA, Planquette B, Rivet N, Jourdi G, Hauw-Berlemont C, Hermann B, Gaussem P, Mirault T, Terrier B, Sanchez O, Diehl JL, Fontenay M, Smadja DM. Circulating Von Willebrand factor and high molecular weight multimers as markers of endothelial injury predict COVID-19 in-hospital mortality. *Angiogenesis* 2021;**24**(3): 505–517.
53. Cugno M, Meroni PL, Gualtierotti R, Griffini S, Grovetti E, Torri A, Lonati P, Grossi C, Borghi MO, Novembrino C, Boscolo M, Uceda Renteria SC, Valenti L, Lamorte G, Manunta M, Prati D, Pesenti A, Blasi F, Costantino G, Gori A, Bandera A, Tedesco F, Peyvandi F. Complement activation and endothelial perturbation parallel COVID-19 severity and activity. *J Autoimmun* 2021;**116**:102560.
54. Dupont A, Rauch A, Staessens S, Moussa M, Rosa M, Corseaux D, Jeanpierre E, Goutay J, Caplan M, Varlet P, Lefevre G, Lassalle F, Bauters A, Faure K, Lambert M, Duhamel A, Labreuche J, Garrigue D, De Meyer SF, Staels B, Vincent F, Rousse N, Kipnis E, Lenting P, Poissy J, Susen S, Lille Covid Research Network (LICORNE). Vascular endothelial damage in the pathogenesis of organ injury in severe COVID-19. *Arterioscler Thromb Vasc Biol* 2021;**41**:1760–1773.
55. Berger JS, Kornblith LZ, Gong MN, Reynolds HR, Cushman M, Cheng Y, McVerry BJ, Kim KS, Lopes RD, Atassi B, Berry S, Bochicchio G, de Oliveira Antunes M, Farkouh ME, Greenstein Y, Hade EM, Hudock K, Hyzy R, Khatri P, Kindzelski A, Kirwan BA, Baumann Kreuziger L, Lawler PR, Leifer E, Lopez-Sendon Moreno J, Lopez-Sendon J, Luther JF, Nigro Maia L, Quigley J, Sherwin R, Wahid L, Wilson J, Hochman JS, Neal MD, ACTIV-4a Investigators. Effect of P2Y12 inhibitors on survival free of organ support among non-critically ill hospitalized patients with COVID-19: a randomized clinical trial. *JAMA* 2022;**327**:227–236.
56. RECOVERY Collaborative Group. Aspirin in patients admitted to hospital with COVID-19 (RECOVERY): a randomised, controlled, open-label, platform trial. *Lancet* 2022;**399**:143–151.